Chapter II

$CuIn_xGa_{1-x}S_2$ Absorber Layer

II.1 Brief History

$CuInS_2$ (CIS) compound was first synthesized in 1953 by Hahn and co-workers [48]. Later Wagner *et al.*, 1975 proposed it as a PV absorber material by demonstrating a working solar cell with PCE 12% by evaporating n-type CdS onto p-type monocrystalline CIS (Bell Laboratories, USA) [49]. Even though Wagner et al. demonstrated the efficiency of CIS, which was quite comparable to c-Si in 1975, the development was hindered by the difficulty in growing high-quality single-crystal CIS. In 1976, thin-film CIS solar cell was fabricated with an efficiency of ~5% by evaporating CIS powder in the presence of excess Se vapor [50]. In 1977, Kazmerski *et al.* reported copper indium sulfide thin-film homojunction solar cells with an efficiency of 3.62% [51]. Later, in 1981, the CIS-based TFSCs started receiving greater attention when Mickelsen *et al.* established efficiency of 9.4% by using co-evaporation of the elemental source. In 1984, a cell with ~11% efficiency was demonstrated at Boeing Corporation using the three-source co-evaporation process of Cu, In, and Se [52]. In the late 1980s, Arco Solar, a USA based company, reported efficiencies as high as ~14% with a two-step process using Cu and In metallic precursors. Later, sodium doping was found to further enhance the performance [53]. The first commercial CIGS solar modules were produced by Arco Solar in 1988 [54]. A series of improvements in the basic solar cell

configuration was made by Boeing that led to improved performance of the CIS TFSCs solar cells. Following important modifications were made at Boeing corporation:

1. Increasing the bandgap from 1.02 eV($CuInSe_2$) to 1.1-1.2 eV by the partial substitution of Ga for In [55],
2. The undoped CdS and a TCO (ZnO) (≤50 nm) were used in place of the 1-2μm thick doped (Cd, Zn)S current-carrying layer [56] resulting in increased short circuit current,
3. Replacing the borosilicate substrate with the soda-lime glass (SLG), which improved the device performance because of the diffusion of sodium from SLG to the absorber layer [57], and
4. Introducing bandgap gradients as a function of thickness [58, 59].

Current Status

The highest reported PCE of CIGS solar cell is ~24% by Solar Frontier, Japan [20]. Several companies worldwide are pursuing the commercialization of $Cu(InGa)Se_2$-based modules, with Ms Shell Solar Industries (SSI), Solar Frontier being the leaders. Good reproducibility has been demonstrated in module manufacturing using the two-stage selenization process for $Cu(InGa)(S, Se)_2$ deposition [3]. SSI now produces commercial modules with 5, 10, 20, and 40 W ratings. Recently, Wurth Solar (Germany) has begun pilot production of large area modules (with an efficiency of ~12%) utilizing an in-line co-evaporation process for $Cu(InGa)Se_2$ deposition.

II.2 Device Structure

The CIGS solar cell is a heterojunction device comprising of several different layers. The most successful device architecture is SLG/Mo/CIGS/CdS/i-ZnO/Al-ZnO/Ni-Al, which was first fabricated at Boeing [52]. SLG substrate is the most commonly used substrate. Molybdenum (Mo) layer (~500 nm) is deposited over the SLG, which acts as the hole collector and light reflecting back contact. A p-type CIGS absorber layer is deposited on the top of the Mo film followed by the deposition of a CdS buffer layer (~70 nm), which is an n-type material and forms a p-n junction with CIGS. Subsequently, a thin (~ 50 nm) high resistance i-ZnO is deposited on top of the CdS layer, followed by the deposition of Al-doped ZnO film (~ 250 nm) [60], which transports the photo-generated electrons. At the top, the Ni-Al electrode is deposited for collecting the current. The function of each layer is discussed in the following sub-sections.

Soda-lime Glass Substrate

The essential feature of the substrate is to act as a base and provide mechanical stability to the solar cell. In the early days, ceramic and borosilicate glass substrates were utilized, which has now been completely replaced by the low-cost, soda-lime glass (SLG) substrate. SLGs have a matching thermal expansion as that of CIGS (9×10^{-6}/K) while Na present in SLG diffuses during selenization/annealing into the CIGS layer which has been shown to improve the performance of CIGS absorber layer [53,61] . The matching thermal expansion coefficient ensures stress free layers and helps in avoiding the formation of voids and microcracks during processing when the films are heated to temperatures as high as 550 °C [62]. In addition, the

diffusion of Na from SLG into CIGS passivates positively charged traps, promote preferred orientation (112) and grain growth in CIGS films during processing [63–66].

Molybdenum Back-contact

The first layer which is deposited over the SLG substrate is the conducting molybdenum (Mo) films of thickness 0.5-1 μm, which act as the hole collecting electrode. Other electrodes materials such as Pt [67, 68], Au [69, 70], Ag [69], Cu [69], and Ni [71] have been tried with mixed results. The Mo film deposited by sputtering is the most suitable candidate for back contact, mainly because of its inertness, high conductivity, stability at working/processing temperature (<550 ^{o}C), and low contact resistance [72]. To achieve high efficiency in CIGS-based TFSC, Mo electrode should have high adhesion and conductivity [73]. Generally, the bilayer deposition process is used [74], where a thin layer is first deposited at higher pressure to achieve good adhesion, while the subsequent layers are deposited at a lower pressure to ensure high conductivity. A thin layer of $MoSe_2$ forms during the selenization of CIGS films at the Mo/CIGS interface, which aids in creating an ohmic contact with the device [75, 76]. In addition, $MoSe_2$ tends to promote the formation of large grains within the CIGS, enhancing device performance [77, 78]. The Mo layer with a thickness of ~1 μm typically has a sheet resistance of 0.1 to 0.2 Ω/cm^2 [79].

Cadmium Sulfide (CdS) Buffer Layer

As the absorber layer is illuminated, in CIGS electron-hole pair is generated, however, in the absence of a field/driving force the charge pairs would recombine.

When an n-type layer is deposited on top of the p-type CIGS absorber layer, p-n junction forms, creating an internal electric field that provides the driving force for the change separation. The n-type layer (also known as buffer layer) must have a wider bandgap to allow the incoming photon through it and get absorbed at the absorber layer. At the same time, buffer layer should have a higher n-type carrier concentration to extend the space charge region (SCR) width well into the absorber layer in order to ensure charge separation throughout the absorber layer [80, 81]. Cadmium sulfide (CdS) is a wide bandgap semiconductor (bandgap ~2.3 eV) [82] with an n-type character due to the presence of sulfur vacancies and cadmium interstitials that generally occur during processing [83]. The n-type charge carrier density in CdS is typically ~10^{16} cm^{-3} [84]. It was reported that CdS coating also passivates the defect states such as V_{Se} and V_{Cu} at the CIGS surface and helps to improve the cell performance [85]. Chemical bath deposition (CBD) [82], Spray pyrolysis (SP) [86], closed spaced sublimation(CSS) [87] and RF sputtering [88] are some of the popular CdS layer deposition techniques with CBD being the most widely used method.

Window Layer and Top Contact

In order to collect the electrons at the buffer layer, an electron collector is needed. Placing a metal contact over the whole of the device would allow maximum carrier collection; however, this would shadow the entire device, stopping any incident photons from reaching the absorber. This can be solved by utilizing a transparent conducting window layer [80]. Intrinsic ZnO (i-ZnO) (3.24 eV) and aluminium (Al) doped-ZnO (3.5 eV) are the most popular window layers. The presence of pinhole/cracks in CdS film will form the shunt path from the absorber layer. A thin

layer of resistive and transparent i-ZnO layer blocks any potential shunt path while the highly conductive Al doped-ZnO layer allows the electrons to be transported to the metal electrode. The presence of a thin i-ZnO layer improves the open-circuit voltage (V_{OC}) and fill factor (FF) by reducing the shunt paths. In addition, the i-ZnO layer forms a cliff-like conduction band alignment with the CdS buffer layer and makes the photogenerated electron from the CIGS absorber move to front contact effectively. A thicker (~200 nm) layer of Al-ZnO deposited by sputtering on the top of the i-ZnO serves as the main electrical conductor for generated photoelectrons. Finally, the top contact should have a low contact resistance to the window layer, most popular being Ag, Au and Al/Ni, lines deposited by the thermal evaporation.

II.3 Structural Properties of $CuIn_xGa_{1-x}(S, Se)_2$ Absorber Layer

The progress of CIGS TFSCs over the year and device structure is discussed in sections II.1 and II.2, here in this section, we are going to discuss crystal structure, the phase diagram of Cu-In-S and Cu-In-Se system and band diagram with the interface of CIGS/CdS.

II.3.1 Crystal Structure

$CuIn(S,Se)_2$ exhibits three crystallographic polymorphs: wurtzite (hexagonal), zinc blende (cubic), and chalcopyrite (tetragonal) as shown in **Figure II.1** [89]. Wurtzite $CuInS_2$ **(Figure II.1(a))** can be obtained by replacing Zn^{2+} cation sites with equal proportion of a lower valence Cu^{+} and a higher valence In^{3+} in wurtzite ZnS randomly without disturbing the S^{2-} sites. Zinc blend on the other hand is based on FCC lattice, where S anions occupy the regular FCC position, while the metal ions

(Cu and In) randomly occupies the tetrahedral voids (¼, ¼ ,¼) positions **(Figure II.1(b))**. Chalcopyrite phase can be obtained when two zinc blend unit cells are stacked one over another (along 001) with Cu and In occupying Zn sites in an ordered manner resulting in tetragonal symmetry (space group $I\bar{4}2d$ (No.122)). Therefore, in chalcopyrite structure, each S/Se anion is coordinated by two Cu^{+} and two In^{3+} cation's while each cation is tetrahedrally coordinated by four anions. The lattice parameter *c*, along [001] direction, of zincblende (zb) is close to half of the chalcopyrite (ch) phase, while the lattice parameter *a* (along [100]) is almost equal to that of phase **(Figure II.1(c))**. Out of the three polymorphs, chalcopyrite $CuIn(S,Se)_2$ is the thermodynamically stable polymorph at room temperature.

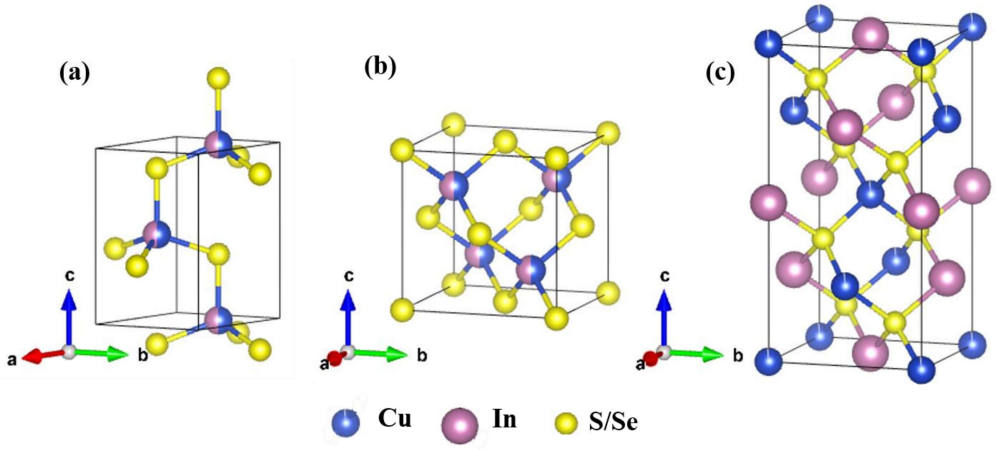

Crystal Structure	Hexagonal	Zincblende	Tetragonal
Space Group	P63mc(186)	F-43m(No.216)	I-42d (No. 122)
Lattice Constant	a=b=3.908Å c=6.427Å	a=b=c=5.523Å	a=b= 5.523Å c=11.133Å

Figure II.1 The unit cell of the polymorphs of $CuInS_2$: (a) Wurtzite (b) Zincblende (c) Chalcopyrite.

II.3.2 Phase Diagram

Cu-In-S System

In 1980, Binsma et. al. [89] published the tentative pseudo binary phase diagram of Cu_2S—In_2S_3 as shown in **Figure II.2(a)**. Here, γ-phase is the chalcopyrite $CuInS_2$ (which is stable up to 980 °C), δ-phase is having the zincblende structure (stable in the temperature range 980 to 1045 °C) while the ζ-phase has the wurtzite structure which is thermodynamically stable above 1045 °C up to the melting point 1090 °C. Another compound $CuIn_5S_8$ has a spinel structure with melting point 1085 °C [89]. Chalcopyrite to zincblende phase transition in $CuInS_2$, takes place at 980 °C with disordering of the cation sublattice (In^{3+} and Cu^{+}). Wurtzite CIS which is metastable at room temperature was first synthesised by Pan *et al.* [44].

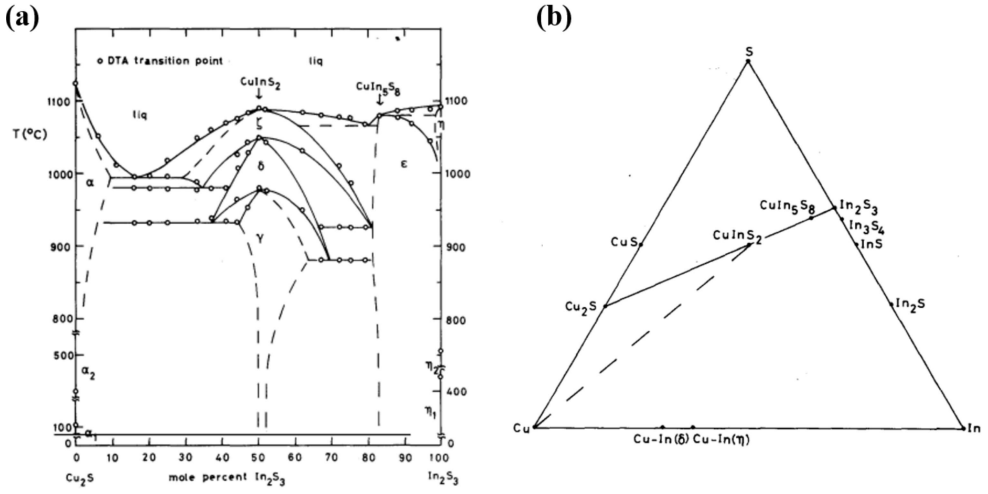

Figure II.2 (a) Pseudobinary phase diagram Cu_2S–In_2S_3, the Phase diagram of Cu-In-S system, (b) Gibbs phase triangle of the system Cu–In–S. Adapted from Ref [89].

Figure II.2(b) shows the Gibbs phase triangle for Cu-In-S system with the binary (Cu_2S, In_2S_3) and ternary ($CuInS_2$, $CuIn_5S_8$) phases. The p-type $CuInS_2$ absorber semiconductor forms with Cu-poor and excesses of S elements. Tolerance to the deviations from stoichiometry is one of the key reasons for Cu(In, Ga)S_2 being such a successful material for thin-film solar cells.

Cu-In-Se System

A pseudo binary Cu_2Se–In_2Se_3 phase diagram is shown in **Figure II.3(a)** [90]. The α-$CuInSe_2$ phase which has a chalcopyrite crystal structure, is thermodynamically stable from room temperature (RT) to 810 °C [91]. The α-phase occurs over a very narrow composition range from 24 to 24.5 at% Cu at RT while with temperature the composition range increases. At 500-550 °C, the stable α-phase composition range is from 22-24 at% Cu. The δ-$CuInSe_2$ phase is stable at a temperature above 800 °C and it can be constructed by disordering the cation sub-lattice (Cu, In), which leads to the zinc blende structure. β-$CuIn_3Se_5$ phase which is an In-rich phase, is usually referred to as an "ordered defect compound" (ODC) built by ordered arrays of defect pairs (Cu vacancies (V_{Cu}) and In_{Cu} (anti-site defects)). It is also called the "ordered vacancy compound" (OVC) [92]. The Cu_2Se phase, on the other hand, is similar to the β-phase, being constructed from the chalcopyrite structure by introducing Cu interstitials and Cu_{In} anti-sites. Another line compound γ-$CuIn_5Se_8$ becomes stable on further moving towards the indium rich composition. Unlike Cu_2S-In_2S_3, wz-$CuInSe_2$ is a metastable phase, which has been reported by various researchers [93–95]; however, it does not appear in the pseudo binary Cu_2Se-In_2Se_3 phase diagram. **Figure II.3(b)** shows a ternary elemental phase diagram of Cu, In and Se at RT [96]. The p-type $CuInSe_2$ absorber grown with an excess supply of

selenium has a composition on or near the tie line of Cu_2Se and In_2Se_3. It is interesting to note that the ODC lie on the same tie line with a similar chalcopyrite structure. The partial substitution of Ga in place of In and diffusion of Na from SLG suppresses the formation of ODC and expands the α-chalcopyrite phase field towards the Cu poor composition. For the $Cu(In_xGa_{1-x})(S,Se)_2$ TFSCs, the most suitable phase is chalcopyrite (α-phase) with which efficiencies >20% has been achieved [20].

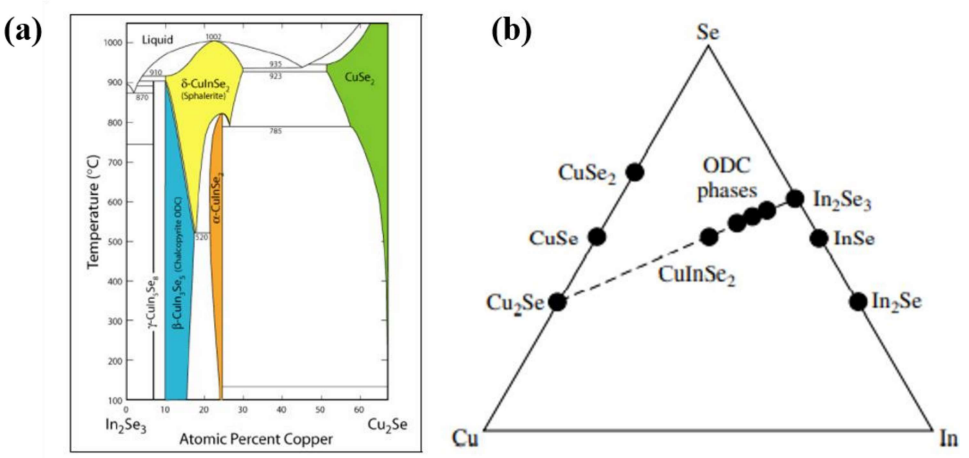

Figure II.3 (a) Pseudobinary phase diagram Cu_2Se–In_2Se_3, Phase diagram of Cu-In-Se system, (b) Gibbs phase triangle of Cu–In–Se system at room temperature. Adapted from Ref [96].

II.3.3 Defects in $CuIn_xGa_{1-x}(S, Se)_2$

A high performance p-type $CuInSe_2$ is obtained if the material is slightly Cu-poor ([Cu]/([Ga]+[In]) in the range of 0.8–0.9) [97, 98]. On the other hand, an overall Cu-rich film with selenium deficiency results in n-type $CuInSe_2$, here vacancy of Se (V_{Se}) is responsible as the dominant donor in p-type film. The energy levels

associated with the V_{Cu} and V_{Se} are close to the valence (resembling the acceptor level) and conduction bands (resembling the donor level), respectively. Relatively deeper anti-site In_{Cu} defect also forms in the presence of V_{cu}. Zhang *et al.* demonstrated that the formation energy of defects complex $2V_{Cu}+In_{Cu}$ is close to zero or negative, depending on the chemical potential [99]. This means that the defect pair of $2V_{Cu}$ and In_{Cu} exits spontaneously under equilibrium conditions in abundance especially in Cu poor compositions. The formation of such defect complexes might be the main cause of the formation of ODC ($Cu(In,Ga)_3Se_5$ and $Cu(In,Ga)_5Se_8$) in the Cu-poor compositions. In addition, the defect complex pairs are electrically inactive due to the passivation of In_{Cu} deep level by $2V_{Cu}$ [100–102]. The defect formation energy of single acceptor defects (V_{Cu}, V_{Ga}, and Cu_{Ga}) in $CuInSe_2$ and $CuGaSe_2$ are similar [99] while the formation energy of single donor defects (such as Ga_{Cu}, Cu_i) is greater in $CuGaSe_2$ than in the case of $CuInSe_2$. The large formation energy of the donor defects in $CuGaSe_2$ is primarily due to the fact that the substitution of Ga for In increases the bandgap by shifting the conduction band to higher energies. As a result, the acceptor transition levels in $CuGaSe_2$ and $CuInSe_2$ are at similar level; however, Ga_{Cu} donor level in $CuGaSe_2$ are much deeper than the In_{Cu} donor level in $CuInSe_2$. This makes the formation of $(2V_{Cu}+Ga_{Cu})$ defect pairs much more difficult in $CuGaSe_2$. The unpassivated Ga_{Cu} defects act as electron traps in Ga-rich $CuInGaSe_2$ compounds[99]. Therefore, to obtain high efficiency in $CuIn_xGa_{1-x}Se_2$ solar cells, Ga/(Ga+In) ratio is kept close to 0.3, while Cu/(Ga+In) ratio is generally from 0.8-0.9 [79]. It has later been demonstrated that an increase of the Cu content toward stoichiometry tends to lower Urbach energies (used to quantify energetic disorder in the band edges of a semiconductor), lower defect density, improved carrier transport, increased optical

absorption and improved crystallinity [103–106]. However, CIGS solar cells with increased Cu contents typically have lower performance [107, 108] mainly due to the formation of Cu_xSe secondary phases in the surface region [109].

II.3.4 Band Diagram and Interface of CIGS/CdS

The CIGS solar cell structure consists of several layers including the top and back contacts as depicted in **Figure II.4(a)** while each layer has different bandgap and electron affinity. The chalcopyrite CIGS absorber layer has a bandgap (E_g) in the range of 1.02 to 1.67 eV, depending up on y = (GGI) = [Ga]/([Ga] + [In]), where y ranges from 0 to 1 [110]. The broadening of E_g primarily occurs by up-shifting the minima of the conduction band. The following equation gives the variation of CIGS E_g as a function of y, which was derived by fitting the experimental data [111]:

$$E_g = 1.01 + 0.42y + 0.24y^2$$

Variation in the GGI ratio across the absorber layer gives rise to the bandgap grading. There are a different forms of bandgap grading: back, front and double grading [112]. Back grading is defined as an increase in E_g going toward the back (Mo side) of the absorber layer, whereas in the case of front grading E_g increases on approaching the front (towards CdS buffer layer) of the absorber. On the other hand, in double grading minimum E_g is somewhere midway which is known as notch. Each type of grading has its own advantage. A back grading enhances the collection of minority carriers and reduce back contact recombination while front grading improves V_{OC} due to broadening the E_g in the SCR [113]. Double grading allows for increased device performance by achieving a high J_{sc} by promoting

absorption of low energy photons, increasing V_{oc} due to the locally increased E_g in the SCR [114].

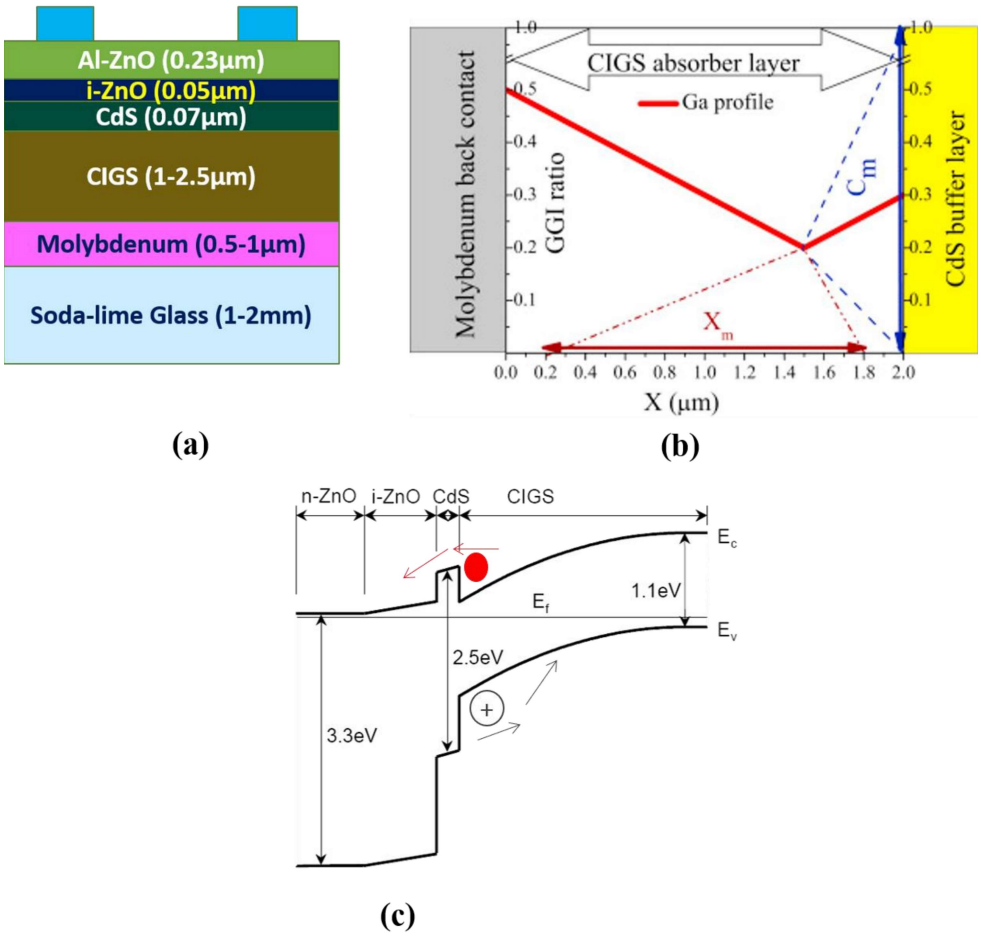

Figure II.4 (a) Typical architecture CIGS solar cell, (b) Ga content profile of the CIGS absorber layer used in simulation (The blue and brown arrows show the ranges of C_m ((middle of CIGS absorber layer) and X_m (different distances from back contact)) respectively, Adapted from Ref [113]), (c) Energy band-diagram of a CIGS solar cell with p-type absorber/n-type buffer/n-type window structure between two metallic contacts after.

Typically, the notch of the gradient profile should be very close to the SCR so that the generated carriers can be swept across under the influence of the electric field at the junction **(Figure II.4(b))** [113, 115]. There are various reports discussing the ideal grading profile based on computer simulations [113, 116, 117].

The CdS buffer layer has $E_g \sim 2.4$ eV while the E_g of the window layers is around 3.2 and 3.5 eV for i-ZnO and Al-ZnO, respectively. When these are stacked, alignment of the Fermi level takes place leading to carrier diffusion across the interface between the p-type CIGS absorber and n-type CdS buffer layer which causes bending of the valence and conduction bands and an internal field which opposes the diffusion, as shown in **Figure II.4(c)**. The depletion region formed through the buffer layer and extends up to a several hundred nanometres into the CIGS absorber layer. An incident photon with energy larger than the CIGS bandgap ($E_{ph}>E_g$) is generally absorbed within 1-2 μm of the absorber layer, generating electron–hole pairs that are spatially separated by the internal electric field at the p–n junction which push the electrons towards n-type buffer layer and gets collected though the Al doped ZnO at the line electrode, while the holes are pushed towards the Mo hole collector.

One of the key parameters in the band alignment is the conduction band offset (CBO) which is defined as the energy difference (ΔE_C) between conduction band minima of the buffer (CdS) and absorber (CIGS) layers. CBO (ΔE_C) can be estimated using the ultraviolet photoelectron spectroscopy (UPS) [118, 119]. The positive value of CBO creates a spike, which impedes the flow of electrons from the p-type absorber to the n-type buffer layer. Theoretically, values $0 \leq \Delta E_C \leq 0.4$ is suitable to ensure effective charge separation. This spike creates a local n-type

inversion and increase the width of depletion region (SCR), subsequently shifting the SCR towards CIGS side, and inturn decreases the recombination at the CISG/CdS interface, enhancing the performance of the solar cell. If CBO is negative, a cliff arises in the band structure that will promote the recombination and degrade the device performance. A recent report shows that Cd-free buffer layers, such as ZnS, one of the main problem is the large CBO of the order of 1-1.2 eV between the conduction band minimum of buffer and that of CIGS [120]. A higher spike obstructs the flow of electrons from the absorber to the buffer side, reducing the J_{sc} and FF. Therefore, the CBO at the absorber/buffer interface needs to be controlled.

II.4 Deposition Techniques for CIGS Absorber Film

A wide range of deposition approaches demonstrated for processing of CIGS absorber layer, including physical vapor deposition (evaporation and sputtering) and solution based processing. These deposition techniques can be divided into two broad categories viz. vacuum based and non-vacuum techniques. Lab-scale fabrication focus on precise control over the CIGS film composition and cell efficiency. On the other hand, for the large-scale production apart from delivering high efficiency, the processing should be reproducible, high-throughput, tolerant to small deviations, and most importantly cost effective. In the following section, common CIGS layer processing techniques and their advantages are discussed.

II.4.1 Vacuum-based Deposition Techniques

Co-evaporation and sequential deposition are the two most popular vacuum-based deposition techniques for CIGS absorber films. In co-evaporation elements are

evaporated together to achieve uniform elemental distribution over the film volume which on annealing forms CIGS. On the other hand, in sequential deposition process metallic elements (Cu, In and Ga) are deposited in layers, which is later annealed in H_2S or H_2Se between 450 and 600 ^oC to form CIGS absorber layers. Vacuum-based deposition techniques are attractive due to their controlled stoichiometry and potential for achieving high uniformity in lab-scale or sub-models. However, the installation and maintenance cost of these techniques are quite high which restricts their large-scale implementation.

Co-evaporation

The thin-film CIGS-based solar cells have demonstrated efficiencies >20% consistently, where the CIGS absorber films were prepared by the co-evaporation method [20, 121–123]. The thin film is deposited by evaporating Cu, In, Ga, and Se from elemental sources as shown in **Figure II.5(a)**. To achieve the required film composition and composition gradient, precise control of elemental evaporation rates is necessary. Generally, an electron impact emission spectrometer (EIES), atom absorption spectrometer (AAS) or mass spectrometer (AMS) is used for monitoring of elemental evaporation. The deposition is carried at substrate temperatures around 300-550 °C. There are several variants of co-evaporation [124–127], however, the best absorber films with most favoured elemental concentration gradient are deposited by the inverted three-stage process [128]. It promotes the collection efficiency of photogenerated electrons and a higher V_{OC} of the solar cell having a V-shaped Ga gradient **(Figure II.4(b)).** A schematic of the inverted three-stage processing is depicted in **Figure II.5(b)**.

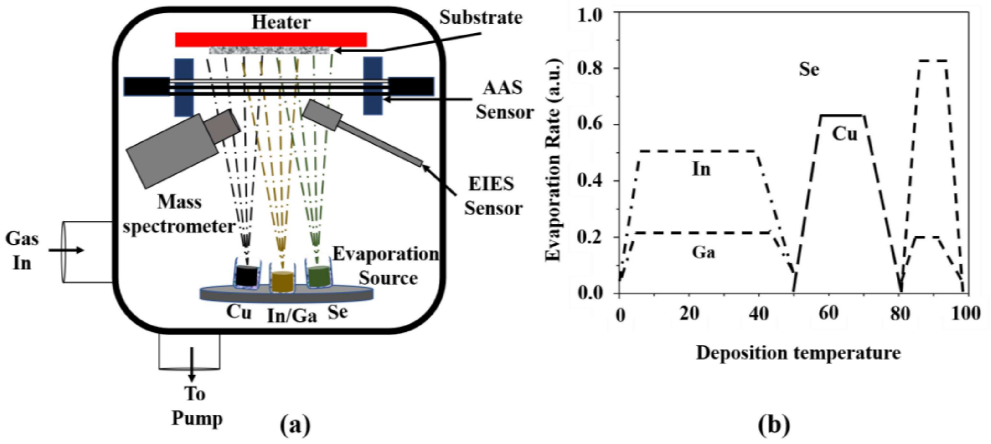

Figure II.5 (a) Schematic setup of the co-evaporation process, (b) Three stage process in which In and Ga are deposited in the first and third stage, whereas Cu is deposited in the second stage.

In the first stage, In, Ga, and Se are evaporated to get $(In, Ga)_2Se_3$ at 300 °C on the substrate. In the second stage, Cu and Se are evaporated and deposited on the substrate at elevated temperature ~550 °C, while during the third stage, In, Ga, and selenium are evaporated again. The In and Ga are deposited in the third stage to ensure the In-rich/Cu-poor composition is closer to the buffer layer. A graded Ga/In profile is also employed in the three-stage process, indirectly it is a combination of Cu-poor, Cu-rich and graded Ga/In profile [118]. The inverted three-stage process leads to smoother film morphology, which reduces the junction area, intern expected to minimize defects at the junction [119] and obtain high efficiency solar cells. Recently, modified 3-stage process with several sub-stages of varying evaporation rates of In and Ga has been reported [129–131] with highest reported cell efficiencies of 20.8% [117].

Sequential Deposition

The second technique to make CIGS layer is the sequential process or two-step process using magnetron sputtering as shown in **Figure II.6(a)**. There are two different approaches with respect to the selenization of the thin film. The first approach, selenization is carried out using H_2Se vapor as source during annealing **(Figure II.6(b))**.

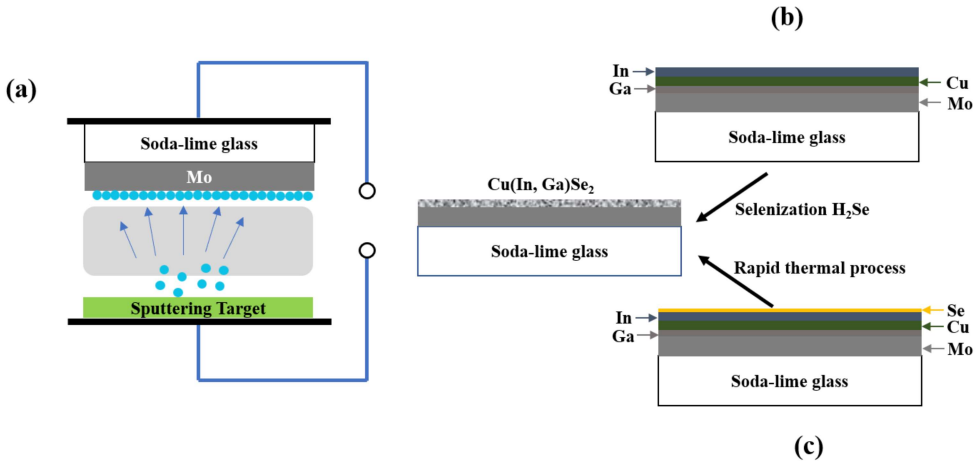

Figure II.6 (a) Schematic set-up of the sputtering system, Two-step process (sequential selenization), (b) Selenization from the vapor of H_2Se, (c) Selenium evaporation and a rapid thermal process (RTP) in an inert atmosphere.

In this, the Cu, In and Ga layers are deposited on Mo coated SLG by sputtering. The deposited layers are selenized at ~500 °C in H_2Se atmosphere to achieve CIGSe thin film [132, 133]. The advantage of this approach is scalable to larger area which is a major advantage over the co-evaporation process. However, the toxicity of hydrogen selenide (H_2Se), is a major concern. In the other approach **(Figure II.6(c))**, H_2Se is avoided by depositing Se as the last layer in sequence, which is

annealed in inert atmosphere for the layers to react and form CIGS **(Figure II.6(c))**. [134, 135]. Using a two stage selenization process, the best efficiency ~19.2% has been reported [136].

The vacuum deposition processes are capable of good compositional control and high-quality semiconductor layers. However, it requires high energy input, large capital investments, and operational costs. Additionally, process complexities, and lower material utilization hamper their large scale implementation [137]. On the other hand, solution processing (non-vacuum) techniques are easy to handle, requires much lower capital and operating cost, at the same time, easily implemented on industrial scales. Owing to their high throughput solution-based processing of CIGS absorber layers has received immense attention recently.

II.4.2 Non-vacuum (Solution)-based Deposition Techniques

During the last decade, solution processing has been projected as a potentially viable option for CIGS absorber layer deposition. Chemical bath deposition (CBD) [138], electrodeposition [138, 139], inkjet printing [45], spin coating [15], dip coating [140], doctor blade [141, 142], and spray pyrolysis [28, 143], are some of the variants for the solution based deposition technique. **Figure II.7** schematically represents some of the solution-based deposition technologies. The key benefits of the solution-based deposition techniques over vacuum-based techniques includes: (i) low capital investment and low maintenance cost, (ii) reduced material cost and better material utilization, (iii) low energy input, (iv) high-throughput, and (v) are amenable for roll-to-roll processing.

Solution-based deposition techniques are generally carried out in two steps; solution coating followed by a post-deposition treatment (PDT). The solution can be classified according to the applied deposition techniques or the nature of the precursor ink (i.e molecular precursor or nanoparticle). Typically, in the solution processing, the wet-solution (hereafter referred to as ink) is utilized for coating where metal precursors are dissolved or dispersed in a desired solvent along with surfactants and other stabilizing additives. The ink is then deposited over the SLG/Mo substrate, usually with an intermediate drying step. The film is then thermally decomposed into a compact precursor film, which is then annealed in Se/S or H_2Se vapor to obtain the desired composition.

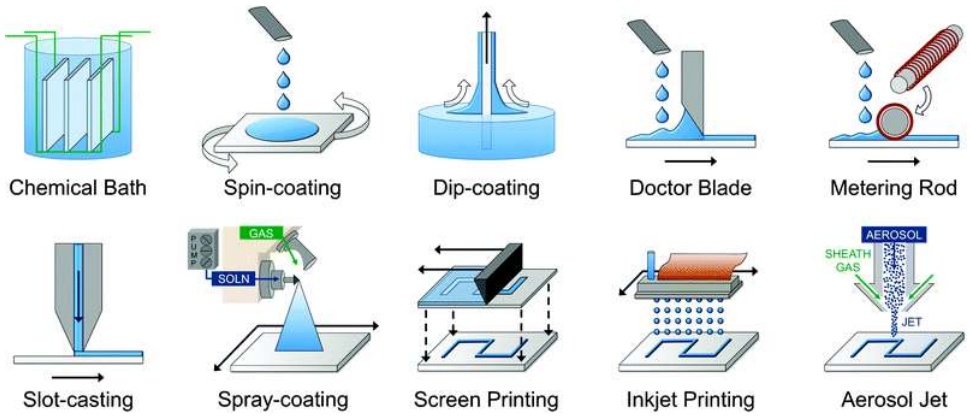

Figure II.7 Number of available solution deposition techniques used for precursor and nanoparticle ink deposition. Reproduced with permission [144]. Copyright 2011, Royal Society of Chemistry.

The challenges associated with solution processing are non-homogeneous, less dense films, and contamination by the unburned precursor. Achieving a uniform, oriented grains over large area and composition gradient along thickness to improve the performance is also challenging [60, 141, 143, 145, 146]. The small grain sizes

introduce more grain boundaries, which tends to trap the charge carriers and thus lower J_{SC}, FF, and contribute a significant loss in efficiency. There are many factors, which restricts formation of dense, large-grained microstructure, including residual contaminants, insufficient annealing, surface roughness, and precursor film porosity [137, 147, 148].

Spray Coating/Pyrolysis

Spray pyrolysis is one of the low-cost deposition techniques, which is easily scalable. Spray pyrolysis have received attention because of being a direct liquid coating process, where a variety of precursor inks can be utilized with minimum requirement of additives. Spray pyrolysis initially became popular in early 1944 for depositing transparent oxide films [81]. In 1966, Chamberlin and Hill extended this method to grow sulfide (CdS, ZnS) and selenide (CdSe) films [149]. Pamplin *et al.* successfully deposited $CuInSe_2$ (zinc blende) onto the glass substrate at 350 ^{o}C (substrate temperature) by spraying mixed solution of 0.02 M cuprous, indium chlorides and N,N-dimethyl thiourea [150, 151]. The highest reported efficiency of CIGS solar cell processed by spray pyrolysis technique is 10.7% [152].

The working principle of spray pyrolysis is straightforward, where an aqueous solution containing soluble salts of the constituent elements of the desired compound is sprayed onto heated substrates. The sprayed droplets, when comes in contact with the hot substrate surface undergo pyrolytic decomposition and form the desired film. Film formation process during spray pyrolysis can be described by the following stages: (1) spraying of aqueous solution, (2) solvent evaporation, (3) drying, (4) thermolysis, (5) formation of microporous particles, (6) formation of

solid particles, and (7) sintering of solid particles [153]. Quality of the film can be easily maintained by controlling the deposition parameters such as precursor flow rate, substrate temperature, nozzle distance from the substrate, nature of additives, and the concentration of reactants in the precursor solution. By utilising more than one dispenser and varying the individual precursor flow, composition of the films can be changed during spray process, resulting in layered films and films having composition gradients throughout the thickness. Similar to other solution techniques incomplete removal of solvents or incomplete decomposition of precursor results in small grain sizes, porous films and trapped impurities. Therefore, careful selection of processing parameters, such as spray composition, substrate temperature, spray head speed and distance, is critical. The detailed description of the spray deposition experimental setup and optimization is discussed in chapter III and chapter VII, respectively.

II.5 Ink-based Solution Processing Routes

Molecular Ink-based Solution Processing Routes

In this processing route, molecular ink is prepared by dissolving metal salts of copper, indium, gallium into volatile solvents. Sometimes additional agent like co-solvents and additives are used. Molecular ink is generally a single-phase homogeneous liquid (true solution), which is directly used to produce films followed by an selenization process (**Figure II.9(a)**). Several solution methods have been developed based on solvent such as water, alcohols, butyldithiocarbamic acid (BDCA), hydrazine, amine–thiols, dimethyl formamide (DMF) and dimethyl sulfoxide (DMSO) and their corresponding record PCE is shown in **Figure II.8**.

Water as a solvent received great attention due to being easily removable during pyrolysis, and inexpensive [154]. As the deposition of the film is generally carried out at temperatures greater than 350 ^{o}C, there is a probability of formation of molybdenum and indium oxides film [60, 142]. PCE as high as 12.3% has been reported with water-based inks [154]. The use of alcohol-based solvents and organic binder materials prevent metal evaporation and segregation. However, the use of alcohol-based solvent leads to trapping of residual carbon in the film especially at the deeper regions closer to the substrate. The trapped carbon also restricts grain growth [155, 156]. CIGS absorber layer spin coated using a precursor solution in methanol has been shown to result in PCE close to 14.4% [36]. BDCA–EtOH was utilized as a solvent by Wang *et al.* to fabricate CIGS-based cells with PCEs as high as 10.1%. A major reason for the cells not realizing high efficiency was attributed to the residual carbon in absorber layers as both of the constituents chemically belong to the $CH_3(CH_2)_3NH_2$ and CS_2 [157]. To mitigate the issue of residual carbon, hydrazine was utilized as a solvent which resulted in a PCE of 18.1% which is a record for any solution processed CIGS-absorber film. However, hydrazine is explosive and toxic, and cannot be adopted in industry for large scale production [33]. Another solvent used is a binary amino-thiol mixture [158], which can dissolve several inorganic materials by adjusting the amine–thiol ratio in the solvent mixture. Using this approach of dissolving metal chalcogenides in ethylenediamine/1,2-ethanedithiol resulted in devices with power conversion efficiency (PCE) 16.4% [159]. Even though the solubility of amino-thiol mixture to some extent matches with hydrazine, both the thiol and amine groups are toxic in nature, which derived the search for alternative solvents such as dimethyl sulfoxide (DMSO), dimethyl formamide (DMF), etc. DMSO and DMF solvents

contain high polarity and an unreactive oxygen site that will rule out the formation of M-O-M or M-O-C bonds, which could be difficult to remove once created [137, 160].

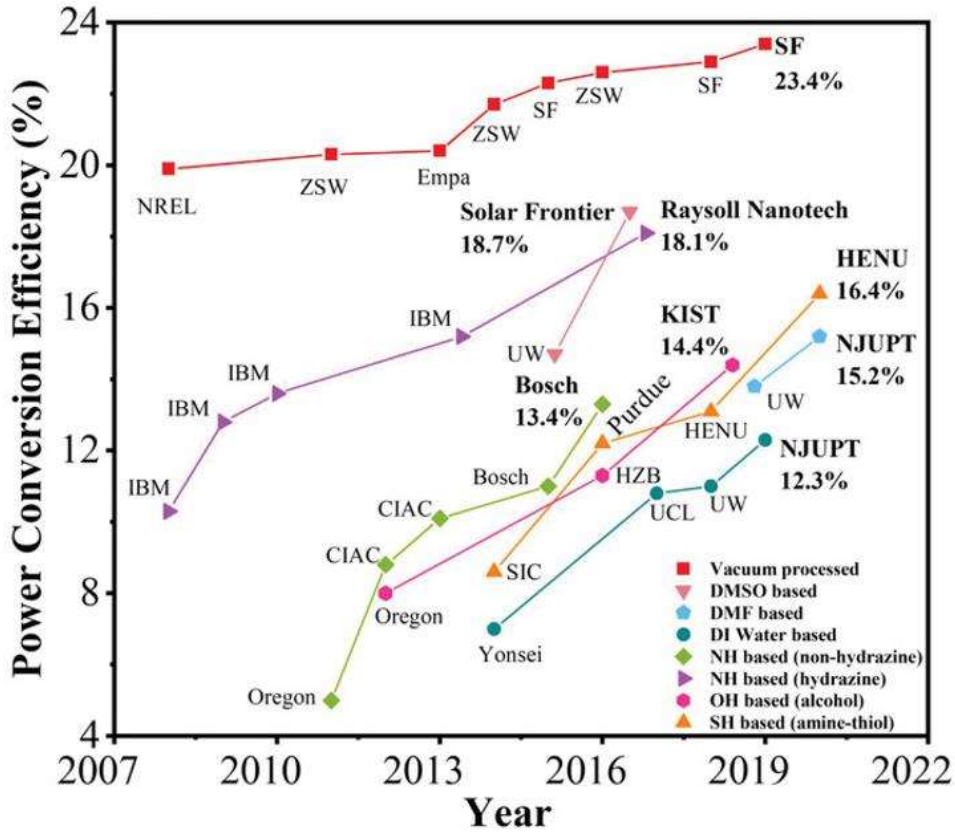

Figure II.8 Evolution of record efficiency $Cu(In,Ga)(S,Se)_2$ solar cells from molecular-ink routes comparing with vacuum-based solar cells shown as a reference. Reproduced with permission [137].

DMSO-based route obtained the highest PCEs of 18.7% for CIGSSe solar cells [35]. It is attractive since it is binder-free, offers effective metal complexing, and contains a high concentration of chalcogen in the ink which could improve spatial uniformity [161]. Despite several advantages, the low solubility of certain metal species (e.g., In^{3+} or Ag^{+}) limits the use of DMSO [15]. DMF has the limit of

solubility of $InCl_3$ from 0.45 to 1.8 M (after initial heating at 120 °C) in Cu–In–S molecular solutions [162, 163]. Utilizing DMF solvent, the highest reported PCEs are 14.5% and 15.2% for CISSe and CIGSSe absorbers, respectively [34]. The selection of solvents is mainly based on their vaporization temperature, flammability and toxicity. Solvents generally add elemental impurities like carbon, chlorine, oxygen, and nitrogen which in many cases are not completely removed during pyrolysis. These trapped impurities adversely affect the absorber quality and electrical characteristics of the film.

Nanoparticle Ink-based Solution Processing Routes

The benefit of the nanoparticle inks over the molecular solutions route lies in the use of non-toxic and easily removable solvent/dispersant. The presence of pre-synthesised nanoparticles having defined structure, and stoichiometry, reduces the possibility of secondary phase formation during post-deposition treatment and offers a range of tunable optical and electrical properties [164]. Nanoparticle ink based processing begins with the synthesis of CIGS colloidal NPs utilizing different synthesis routes such as melt atomization, solvothermal route, salt assisted spray pyrolysis, or hot injection. The synthesized colloidal nanoparticles are washed and dispersed in a liquid media to prepare ink for deposition followed by an annealing process **(Figure II.9(b))**. NPs can be dispersed in a wide range of solvents and stabilizing ligands (e.g., toluene, dodecanethiol, hexanethiol, benzenthiol, dichlorobenzene, oleylamine (OAm), etc.). To effectively extract the generated charge carriers, it is essential to have a large columnar grained microstructure with passivated grain boundaries. During the synthesis of CIGS NPs, low volatile ligands such as oleylamine (BP: 350^{o}C), oleic acid (BP: 360^{o}C), etc. are used to control the

kinetics of nucleation, solvate precursors, and avoid agglomeration. The main benefit of this approach is utilization of ink with a higher mass concentration (>250 mg/ml), which enables formation of dense absorber coating in fewer deposition passes (>800 nm per deposition pass). Lower melting point and higher reactivity of NPs offers the benefits of faster processing at lower temperatures. Highest reported efficiency close to 17.1% demonstrate the potential of NPs ink-based solution processing route.

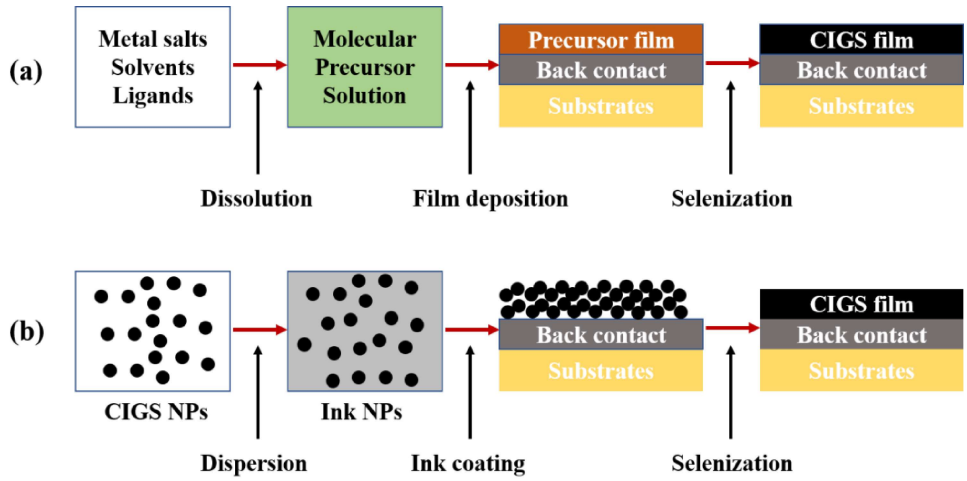

Figure II.9 Schematic diagram comparing (a) the molecular and (b) nanoparticle solution CIGS deposition approach.

Despite the benefits of the nanoparticle ink route, its has its own share of challenges which includes effective washing of pre-synthesised NPs, stabilization of ink, low packing density (which results in voids or pinholes), small grain size, and removal of the dispersant. In addition to that, the organic solvent used such as oleylamine leaves carbon residue that combines with Se and forms the complexes in the fine grain layer during selenization. These issues are addressed in chapter VI.

II.6 Concluding Remarks

The background and current status of CIGS solar cell show their potential among all commercially available TFSCs. Structural correlation between polymorphs of CIGS and their stability regime is discussed. Among the three polymorphs, chalcopyrite is the preferred phase for the absorber layer. The record efficiency of 23.35% has been reported for solar cells fabricated using chalcopyrite CIGS absorber layer deposited using co-evaporation technique. Although highest efficiency cells have been demonstrated with the vacuum deposited CIGS layers, these techniques require high installation and operating cost and are not easily scalable. This has paved way for development of solution-based processing techniques. Spray pyrolysis technique is a promising solution-based processing technique due to low cost, scalability, and control on material wastage. The CIGS layer can be solution processed utilising nanoparticle ink and molecular precursor ink. Nanoparticle ink is preferred in this work mainly to utilize pre-defined structure, and stoichiometry, which also reduces the possibility of secondary phase formation.